π^0 production in $\pi^+ p$ interactions at 10.5 GeV/c *†

J. R. Elliott,‡ L. R. Fortney, A. T. Goshaw, J. W. Lamsa, J. S. Loos, W. J. Robertson, W. D. Walker, and W. M. Yeager§
Physics Department, Duke University, Durham, North Carolina 27706

S. Dhar‖ and C. R. Sun
Physics Department, State University of New York, Albany, New York 12222
(Received 31 May 1977)

Inclusive γ and π^0 production is studied in $\pi^+ p$ interactions at 10.5 GeV/c. The π^0 distributions are compared to those of π^+ and π^- mesons. An examination of the γ-γ mass spectrum confirms the relationship $\sigma(\pi^0) = \sigma(\gamma)/2$ to an accuracy of 10%. π^0 multiplicities and correlations are found to depend only weakly on charge multiplicity; for all inelastic collisions $\langle n_{\pi^0} \rangle = 1.50 \pm 0.05$ and $f_2^{00} = -0.05 \pm 0.06$. The π^+, π^0, and π^- spectra are found to be similar in form when compared differentially in terms of the Feynman x variable. $d\sigma(\pi^0)/dx$ is bounded by the π^+ and π^- cross sections for all values of x.

I. INTRODUCTION

In contrast to the detailed data which exist for charged pions,[1] experimental information on the production of neutral pions in hadronic interactions has accumulated rather slowly.[2] The experiments attempting to study π^0's have been hampered variously by three limitations: (1) reliance upon the single-particle spectrum of γ's, (2) detection of relatively few pairs of γ's from $\pi^0 \to \gamma\gamma$, and (3) acceptance over only a restricted kinematic range. Not every experiment has all three of these difficulties, but the attempt to overcome some of these problems tends to cause compromises which usually introduce the other limitations. This is especially true for a single experiment trying to compare the production of all three pion charge states. In this paper we perform just such a comprehensive analysis of the inclusive production of π^+, π^0, and π^- mesons. The interactions we study are

$$\pi^+ p \to \pi^+ + \text{anything}, \tag{1a}$$

$$\pi^+ p \to \pi^- + \text{anything}, \tag{1b}$$

$$\pi^+ p \to \gamma + \text{anything}, \tag{1c}$$

$$\pi^+ p \to \pi^0 + \text{anything}, \tag{1d}$$

at an incident momentum of 10.5 GeV/c. The use of a hydrogen-neon filled bubble chamber affords an acceptance of photons converting to electron pairs with a reasonably good detection efficiency (20%) for the full 4π solid angle. This provides a large number of single γ's and γ-γ pairs coming from π^0 decays as well as the usual information about charged tracks available in a bubble chamber.

The data acquisition and reduction for the experiment is described in Sec. II. The γ and π^0 inclusive cross sections and the associated moments of their multiplicity distributions are presented in Sec. III. In Sec. IV, γ-inclusive spectra are compared with another experiment at a nearby energy. The possible sources of γ's are considered in Sec. V and the π^0 spectra are extracted from the single-γ distributions. In Sec. VI, the spectrum of π^0's reconstructed from cases where both γ's are detected is compared to that derived in Sec. V. Finally, Sec. VII summarizes the results of comparing the π^+, π^-, and π^0 spectra.

II. EXPERIMENTAL PROCEDURE

A. Event selection

The photographs for this experiment were obtained with a 10.5 GeV/c π^+ beam incident on a hydrogen-neon mixture in the SLAC 82-inch bubble chamber. The neon content was 32.2 molar percent, yielding an interaction length of approximately 400 cm and a radiation length of 125 cm. The film was scanned for events that could have originated from collisions on hydrogen. The properties required for characterizing an interaction as occurring on hydrogen were as follows: (1) no more than one proton identifiable from ionization and range (protons with momenta below 1 GeV/c), (2) +2 net charge outgoing, (3) for identified protons, a minimum projected length of 8 mm (protons with momenta above 160 MeV/c), (4) a proton angle compatible with the recoiling mass of the other charged particles. We will call these events hydrogenlike.

When a hydrogenlike interaction was found, the frame was scanned for associated neutral secondary vertices which were classified as either electron pairs (zero opening angle or identifiable elec-

TABLE I. The numbers of events and γ's used in this experiment. The first sample provided the normalization base for the other two. When appropriate, the samples were combined to reduce statistical errors.

Prongs	Events	Scanned γ's	Final γ's
Cross-section-normalization sample; charged tracks and γ's measured.			
2[a]	2162	1760	1084
4	3433	2244	1444
6	1403	942	605
8	260	166	111
all[a]	7258	5112	3244
Additional sample for inclusive γ study (events with ≥ 1 γ), beam track and γ's measured.			
2	1569	2702	1513
4	2344	3855	2234
Additional sample for π^0 reconstruction (events with ≥ 2 γ's), beam track and γ's measured			
2	2108	5272	2894
4	2865	6986	4018

[a]Inelastic.

tron or positron) or as V^0's (nonzero opening angle, hadron decay or interaction or nonminimum ionization). For the electron pairs the scanners were able to make a good test of vertex association using the initial direction of the tracks at the conversion point. A fiducial limit on the interaction-vertex location ensured a minimum downstream-path length of 60 cm available for γ conversion and V^0 decay.

The event sample consisted of two parts: (1) a comprehensive scan of 56 000 photographs which included all 2-, 4-, 6-, and 8-prong events meeting the hydrogenlike requirements, (2) a restricted scan of 190 000 photographs for hydrogenlike 2- and 4-prong events having one or more associated secondary vertices. The events were measured at Duke on the semiautomatic measuring machine RIPPLE, and at SUNY on a Mangiospago measuring machine. Table I gives a breakdown of the event samples analyzed. The program TVGP was used to reconstruct tracks and to determine their momenta. The final reconstruction efficiencies for charged tracks were about 90% for $\pi^{\pm}$ and 83% for protons in addition to a 15% overall loss of entire events. The scanning efficiencies were determined by an independent scan of 10% of the film and showed an efficiency of $92.7 \pm 1.6\%$ for finding events with a hydrogenlike primary vertex; this figure was nearly independent of the number of prongs.

B. γ processing

γ's were detected in a particularly clearcut manner in this experiment. A consideration of the conversion length of the liquid and the bubble chamber's size gives an average detection efficiency of 20%. The observed sample of γ's was a clean one, and the global visual property of the bubble-chamber technique allowed confirmation that any background or bias was small. Since the detection and measurement of photons converting to electron pairs is the basis of this experiment, we will discuss our analysis procedure in some detail.

As mentioned earlier, the scanning for the electron pairs took place after an interaction vertex was identified; all γ's that could be associated with that beam interaction were then recorded. This visual association of electron pairs is quite reliable because of the small opening angle of the electron-positron pair, although some ambiguities do occur for low-energy pairs. Cases of doubtful association were included in the scan and were left to be resolved on the basis of later measurements. Partial rescanning determined an average scanning efficiency of $93.9 \pm 1.3\%$ for the converting γ's. This was examined in detail with respect to a number of different factors. Specifically, no significant variation could be found as a function of the following: (1) the number of charged tracks, (2) the distance from the interaction vertex (up to 90 cm), (3) the angle of the electron pair with respect to the beam, and (4) the momentum of the electron pair.[3]

The treatment of electrons in a heavy liquid requires one consideration not necessary for hadronic tracks. Since electrons and positrons will undergo bremsstrahlung, it is desirable to limit the track length measured to the minimum needed for a good momentum determination. The optimum measurement length was chosen by combining the usual TVGP estimates of errors due to point setting error and multiple scattering with a bremsstrahlung term calculated using the Behr-Mittner technique.[4] The minimum in the resulting momentum error function was chosen as the cutoff length. For RIPPLE-measured electron pairs, this was done at reconstruction time in TVGP by truncation of the measured points. Templates were used as a quide for the measurements made on the Mangiaspago.

In addition to limiting the track length used for reconstruction, the momentum of an electron or positron was increased to account for the unobserved energy loss from radiation. The Behr-Mittner method estimates a momentum-loss correction by averaging over the known bremsstrahlung spectrum which is cut off in a manner dependent on the minimum change in curvature that can be detected in measurement. This cutoff was determined by centering the π^0 peak of the γ-γ mass distribution on its proper value; a typical correction to a particle's momentum was 5%.

After reconstruction of the electron pair, a point-

ing test was performed by comparing the initial directions of the positron and of the electron with the neutral direction defined by the conversion point and the interaction point. A pointing probability was computed by comparing the difference of these two directions with the expected measurement errors. Electron pairs with too small a probability were rejected; the remaining electrons were reconstructed as γ's by adding the energies of the two tracks and defining the direction as that of the two-point neutral direction. The rejection rate in the pointing test was only 5% of all scanned electron pairs. After this step, physicists examined on the scan table a group of electron pairs including both reconstruction successes and failures as well as pointing rejects. This study indicated that the loss of truly associated γ's due to either faulty geometric fits of the electron tracks or failures of the pointing test was 5%. Furthermore, a background of 1–2% of nonassociated γ's was observed. These effects were independent of the momentum of the converting γ.

A possible source of extraneous electron pairs which still satisfy a pointing cut arises from bremsstrahlung photons radiated from truly associated electron pairs. These bremsstrahlung γ's have two characteristics which can be used for their isolation: (1) an energy lower than the parent electron, (2) a conversion point confined to a well-defined geometic region downstream of the first pair. We developed a technique[5] in which those γ's satisfying the pointing test but converting in the region shadowed by an upstream electron pair were eliminated from the event. This approach also eliminated some nonbremsstrahlung pairs, but the loss could be compensated for by increasing the weights of γ's whose lines of flight would have carried them into the shadow region had they not converted first. This method avoids the difficulty of distinguishing between a primary γ plus bremsstrahlung and the case of two angularly correlated primary γ's. The systematic rejection and reweighting retains the proper weighted number of primary γ's and multi-γ combinations. The primary-γ rejection rate by this technique is only 4%.

Finally, a geometric acceptance probability was calculated for each γ based on its flight path, its cross section for conversion, and the fiducial volume defined for it. This probability is given by

$$P = (X_T/X_{pp})(e^{-l_1/X_T} - e^{-l_2/X_T}), \qquad (2)$$

where

l_1 = the minimum allowed distance from the vertex,

l_2 = the maximum allowed distance from the vertex,

X_{pp} = pair-production length,

X_c = Compton production length,

and

$$X_T = 1/(1/X_{pp} + 1/X_c).$$

The maximum length l_2 was determined by the chamber limits, or the geometric shadow region of another electron pair, or a maximum limit imposed on the separation of the γ from the primary vertex (90 cm for the Duke measurements, 120 cm for the SUNY measurements). A weight equal to the reciprocal of the detection probability was then assigned to each γ; the average value of this weight was 5.0.

All the γ and π^0 cross sections presented later are derived using this weight. In particular we define the inclusive cross section for γ production as $\sigma(\gamma) \equiv \sum_i \sigma_{ev} W_i(\gamma)$. σ_{ev} is the appropriate cross-section weight accounting for all aspects of the event except the γ's. $W_i(\gamma)$, the γ weight, is the inverse of the detection probability obtained from the conversion geometry and processing efficiencies. Specifying the value of a kinematic variable of the γ's determines a differential cross section. Similarly the multi-γ cross sections result if $W_i(\gamma)$ is replaced by the product of the $W_i(\gamma)$'s of the γ's in multi-γ combination.

Several cross checks were performed to search for biases in the final γ sample. The first of these was an examination of the energy partition between the electron and positron. This distribution is predicted by electromagnetic theory, and the data reproduce well the change in shape as a function of γ energy. This makes a particularly good test for the loss of those pairs with one track of extremely low energy. We saw a loss of 7% for very asymmetric pairs ($E_e \pm / E_\gamma < 0.10$) with γ energy below 1 GeV. This loss could come from any of several sources in the electron-pair processing; scanning, measurement, reconstruction, and pointing test. Since corrections are made to the γ sample for all of these reasons and because of the relatively small energy dependence of the loss, no specific additional correction was made.

The calculation of the detection probability of a produced γ is straightforward but of crucial importance to this experiment. A convenient method for checking this is to make a plot in a variable Q_l (defined below), where the conversion distance distribution is remapped into a probability distribution that should be uniform from 0 to 1:

$$Q_l = (e^{-l_1/X_T} - e^{-l_c/X_T})/(e^{-l_1/X_T} - e^{-l_2/X_T}), \qquad (3)$$

where

l_c = the γ-conversion distance.

This was done for each of the planes defining the γ fiducial volume and the plane positions were fixed when a satisfactorily flat distribution was obtained.

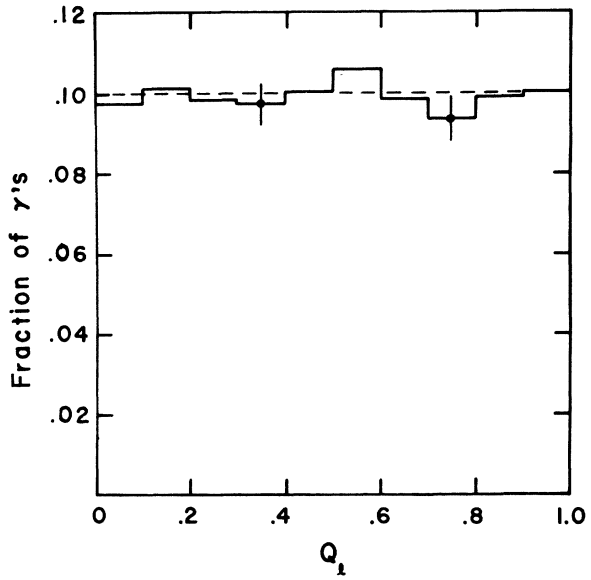

FIG. 1. Probability distribution of the γ-conversion point. As a function of Q_t (see text for definition), this should be constant if γ-detection biases are absent.

Close electron pairs, which might be lost among the primary vertex tracks, and pairs converting far away are two especially sensitive cases that can be examined in this manner, with consequent adjustment of the plane positions. Note that this represents a final check on the entire process. Figure 1 gives the Q_t distribution for all γ's and shows that the geometric cuts are made correctly.

The γ distribution should also be uniform with respect to azimuthal angle (about the beam direction), but the measured sample shows, not surprisingly, some losses of γ's near the camera optical axis. These occur almost entirely for γ's with angles greater than 60° with respect to the beam direction [see Fig. 2(b)]. The Q_t distribution for this category of γ's is shown in Figure 2(a) and reveals losses near the limits of the fiducial volume; i.e., electron pairs converting near the edges of the chamber simply do not have enough projected track length for reconstruction. This represented a 9% correction for γ's with production angles greater than 60° (a 2% correction for the total sample).

C. Cross sections and neon contamination

The cross-section calculation was carried out using the known parameters of the target liquid, the scanned number of incident-beam tracks, and the number of events found. After identification of elastic events and corrections for the scanning losses, the overall result was 35% above the literature value of the π^+p inelastic cross section.[6] Since the

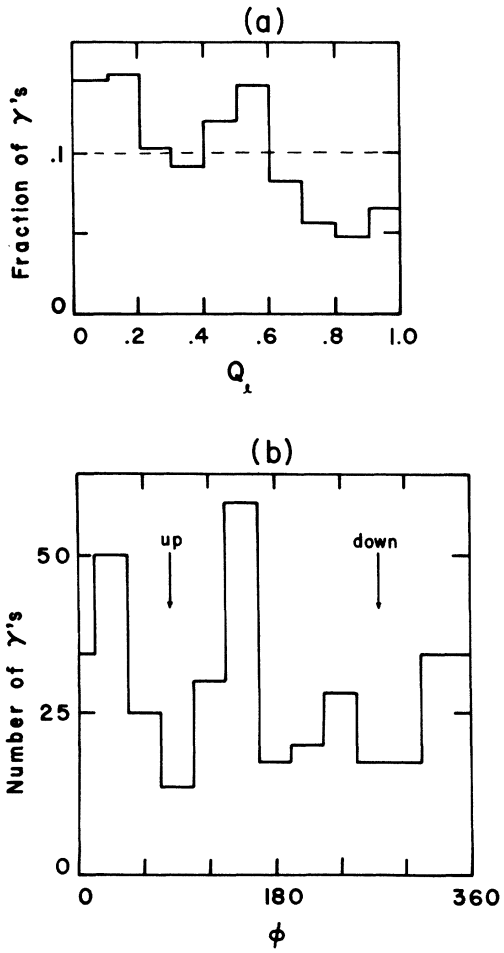

FIG. 2. Properties of γ's detected at an angle $\theta > 60°$ with respect to the beam: (a) Probability distribution of the γ-conversion point showing losses at large Q_t, (b) Azimuthal angle (about beam direction) distribution of γ's showing the loss of γ's produced nearly parallel to the optical axes (up-down) of the cameras.

estimated errors are only 2.3% statistical and 6.4% systematic, the excess events are interpreted as π^+-neon interactions. We note that most π^+-neon interactions are readily distinguishable from π^+-proton interactions at the scan table by virtue of the proton count, excess positive charge, or odd multiplicity. However, a fraction of the π^+-neon events must arise from collisions with a peripheral nucleon, which apart from some initial Fermi momentum tends to act independently from the rest of the nucleus during the collision. Separate studies of π^+-neon collisions have convinced us that the inclusive single-particle spectra produced in these peripheral collisions (with $\lesssim 1$ identified proton) do not differ significantly from those produced in π^+-proton collisions.[7] Therefore the excess events affect only the normalization, and do not

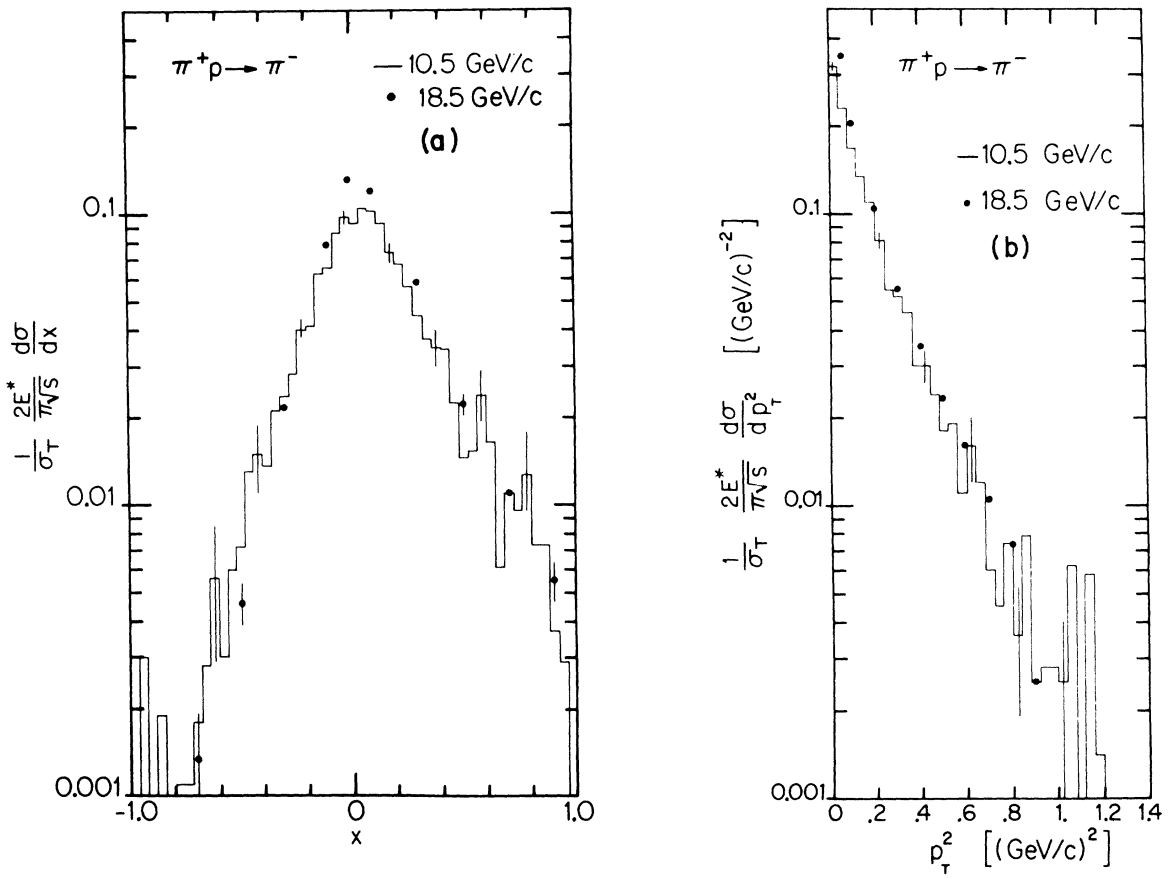

FIG. 3. Invariant differential cross section, divided by σ_T, for π^- production as a function of (a) x and (b) p_T^2 in 10.5-GeV/c π^+p interactions. The solid points are from the 18.5 GeV/c π^+p data of Ref. 9.

seriously distort the π-proton inclusive distributions.

Another method of verifying that our hydrogenlike events have little bias is to directly compare the π^- spectra we obtained with those obtained for a pure hydrogen target at a nearby energy. Figure 3 uses two standard cross sections[8] to display the agreement of our data with $\pi^+p \to \pi^-$ data at 18.5 GeV/c.[9] The plot given in Fig. 4 shows that the distribution in $(1/\sigma_T)E^{1ab}d\sigma/dP$ for π^- also agrees well in the target-fragmentation region, where neon contamination would be expected to appear most strongly.

Our procedure, then, has been to consider the hydrogenlike events to be equivalent to π^+p interactions. Cross-section weights were assigned to each event in order to renormalize to the literature values of topological cross sections. All our results have this normalization included.

III. THE π^0 MULTIPLICITY DISTRIBUTION

In this section we present the general π^0 multiplicity characteristics that can be derived under the assumption that all γ's come from π^0 decays, i.e., $\sigma(\pi^0) = \frac{1}{2}\sigma(\gamma)$. A previous study[10] using a subsample of the present data investigated $\langle n_0 \rangle$, the average number of π^0's observed per event, and $\sigma(n_0)$, the cross section for interactions producing $n_0\pi^0$'s. $\langle n_0 \rangle$ was found to be approximately independent of event charge multiplicity, in contrast to the strong positive correlation observed at higher energies. For all inelastic interactions $\sigma(n_0)$ was determined to be slightly narrower than a Poisson distribution, and its shape was found to be nearly independent of event charge multiplicity.

Present analysis of the total data sample confirms these previously identified features. The results are summarized in Table II which lists $\langle n_0 \rangle$ and f_2^{00} as a function of the charge multiplicity. The second Mueller multiplicity moment $f_2^{00} \equiv \langle n_0(n_0-1)\rangle - \langle n_0\rangle^2$ measures the width of the $\sigma(n_0)$ distribution. The observed average $f_2^{00} = -0.05 \pm 0.06$ (Ref. 11) indicates a slightly narrower distribution than the Poisson shape predicted by independent particle production. Averaging over all inelastic collisions, we find $\langle n_0 \rangle = 1.50 \pm 0.05$.

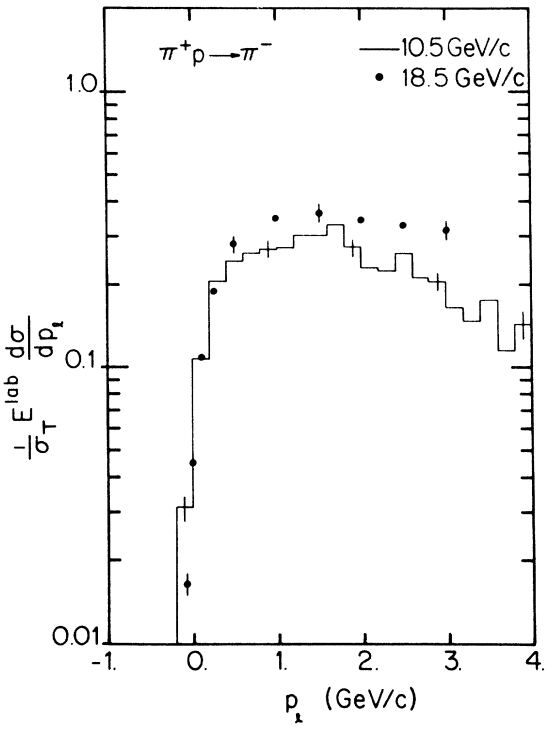

FIG. 4. Energy-weighted laboratory longitudinal-momentum distribution, divided by σ_T, for π^- production in π^+p interactions at 10.5 GeV/c. The solid points are from the 18.5 GeV/c π^+p data of Ref. 9.

IV. INCLUSIVE γ DISTRIBUTIONS

A total of 7000 γ's with complete vector-momentum information are available from our data. In this section we present results based on inclusive studies of these γ's. The sample is fully corrected and weighted to account for the various losses and geometric cuts discussed in Sec. II B.

For the purpose of comparing π^0 production to that of π^+ and π^-, we have generated a large sample of pseudo-γ's using Monte Carlo techniques in which 12 000 π^+ mesons and 4500 π^- mesons undergo a simulated isotropic decay into two γ's. Statistical fluctuations in this process were minimized by simulating several decays for each charged meson. For consistent comparison to γ's from π^0's, these are presented with normalization such that the number of pseudo-γ's, γ_+ and γ_-, is twice the number of source π^+ and π^-. A comparison of the γ_+ and γ_- distribution to those of real γ's allows us to study differences between the π^+, π^-, and π^0 spectra with higher statistics than would otherwise be possible. The assumption that all γ's come from π^0 decays is discussed in Sec. V.

The distribution in the laboratory momentum of the γ's is presented in Fig. 5 and shows a drop of more than three orders of magnitude over the full laboratory momentum range. In Fig. 6, the p_T^2 distribution of the γ's is compared to the γ_- spectrum generated from the simulated $\pi^- \to \gamma_-\gamma_-$ decay. To emphasize the excellent agreement, we have normalized the integrated γ_- cross section to that of the real γ's (in Fig. 6 only). The detailed agreement between the γ and γ_- spectra shows the strong similarity between the shapes of the p_T^2 distributions for π^0 and π^- production. The quantity $F_2(p_T^2)$ is shown in Fig. 7 and agrees well with the results of the Notre Dame (N.D.) $\pi^+p \to \gamma$ experiment at 18.5 GeV/c.[12] Although $F_2(p_T^2)$ is a scaling function, there is evidence from bubble-chamber data in both pp and πp interactions that it does not scale between 10 and 200 GeV/c.[13,14]

The other integrated Feynman scaling function $F_1(x)$ is given in Fig. 8. The agreement with the N.D. data is again quite reasonable. The Fermilab data at 200 GeV/c is not precise enough for a meaningful detailed comparison, however, there is certainly growth in $F_1(x)$ taking place in the interval from 10 to 200 GeV/c.[13,14] If we choose as our variable the center-of-mass rapidity, $y = \frac{1}{2}\ln[(E+P_\parallel)/(E-P_\parallel)]$, we also see the trend reflected in the height of the distribution $(1/\sigma_{inel})d\sigma/$

TABLE II. Topological and inclusive γ and π^0 cross sections, multiplicities, and moments. The hydrogenlike cross sections are our measured values. σ_γ and σ_{π^0} are calculated after renormalizing our data sample to the π^+p cross sections in the literature. The errors listed for σ_γ and σ_{π^0} do not include the uncertainty of the topological cross section.

Prongs	Hydrogenlike σ (mb)[a]	π^+p σ (mb)	σ_γ (mb)	σ_{π^0} (mb)	$\langle n_0 \rangle$	f_2^{00}
2[b]	8.2 ± 0.2	5.5 ± 0.3	19.0 ± 0.7	9.5 ± 0.4	1.73 ± 0.06	−0.31 ± 0.19
4	12.1 ± 0.3	10.0 ± 0.4	27.9 ± 0.9	14.0 ± 0.5	1.39 ± 0.04	0.10 ± 0.14
6	5.3 ± 0.3	3.9 ± 0.2	11.0 ± 0.6	5.6 ± 0.3	1.41 ± 0.07	0.08 ± 0.28
8	1.3 ± 0.2	0.6 ± 0.1	1.8 ± 0.2	0.9 ± 0.1	1.46 ± 0.18	−0.15 ± 1.24
all[b]	26.9 ± 0.6	20.0 ± 0.3	59.7 ± 1.3	30.1 ± 0.6	1.50 ± 0.05	−0.05 ± 0.06

[a] 6.4% systematic uncertainty not included in errors.
[b] Inelastic.

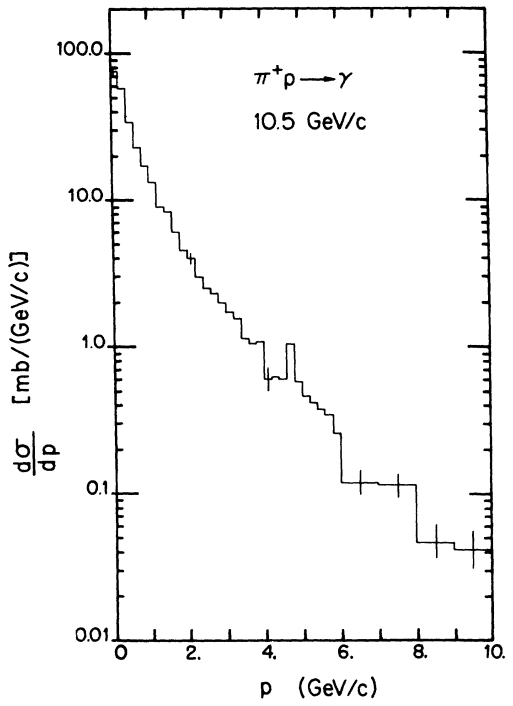

FIG. 5. Laboratory-momentum distribution of γ's produced in 10.5-GeV/c $\pi^+ p$ interactions. This and all other γ distributions are fully weighted as described in the text.

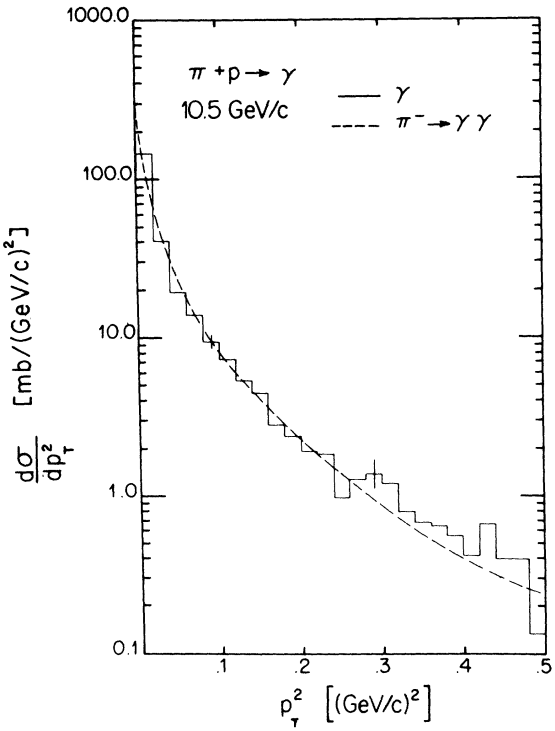

FIG. 6. Transverse-momentum-squared distribution of γ's in 10.5-GeV/c $\pi^+ p$ interactions. The dashed curve represents a Monte Carlo calculation using inclusive π^- production properties in a simulated π^0 decay and is normalized to give the γ inclusive cross section.

$dy|_{y=0}$. Although we already see $d\sigma/dy$ beginning to flatten at $y=0$ in our data (Fig. 9), in both πp and pp interactions a rise of ~30–40% in $(1/\sigma_{\text{inel}})d\sigma/dy|_{y=0}$ occurs from 10 GeV/c through Fermilab and CERN ISR energies.[13,15] We conclude that although the main features of the higher-energy experiments are already evident in our data at 10.5 GeV/c, detailed scaling in the kinematic variables has not yet been attained.

It is worth noting a few points about the γ_+ and γ_- distributions in the figures just discussed. They bracket the actual γ data quite nicely over the entire variable range in both $F_1(x)$ [Fig. 8(b)] and $F_2(p_T^2)$ [Fig. 7(b)] and are not grossly different in shape over a given region. In particular, $F_1(x)$ for γ_+ shows that any leading-particle effect is considerably obscured in viewing only the γ distributions; this is considered later in the derivation of the π^0 spectra.

Our data also show that the $F_1(x)$ distribution of the γ's peaks more sharply about $x=0$ in events of higher charged multiplicity just as it does for π^+ and π^-.[9] Also, a simple factorization of $f(x,p_T^2) = g(x)h(p_T^2)$ fails. This can be seen by plotting $F_1(x)$ for γ's in selected intervals of p_T (Fig. 10). The data for $p_T < 0.100$ GeV/c exhibit a peaking near $x=0$ that is absent in the rest of the data. This effect has also been noted in $\pi^- p \rightarrow \gamma$ at 40 GeV/c.[15]

V. SOURCES OF γ'S AND INCLUSIVE π^0 SPECTRA

A. Sources of γ's

Before discussing measurements of the π^0 spectra, we want to deal with potential sources of γ's. Besides the dominant π^0 decays, there are also η^0 and Σ^0 decays. Another possible source to be considered is the direct production of γ's in some type of bremsstrahlung process occuring when hadrons are created in the primary interaction.[16] Then too, the production of a new unknown particle with a substantial decay mode involving γ's would be an interesting possibility. The most direct and comprehensive approach to this question is the examination of the γ-γ mass spectrum for the π^0 signal. Our use of a hydrogen-neon bubble chamber with a radiation length of 125 cm gives us multi-γ sensitivity over the full angular and kinematic range as well as maintaining acceptable momentum resolutions ($\Delta E/E$ for electrons is typically 8%). Previous experiments[12,17] in hydrogen bubble chambers have found results varying from a π^0 sig-

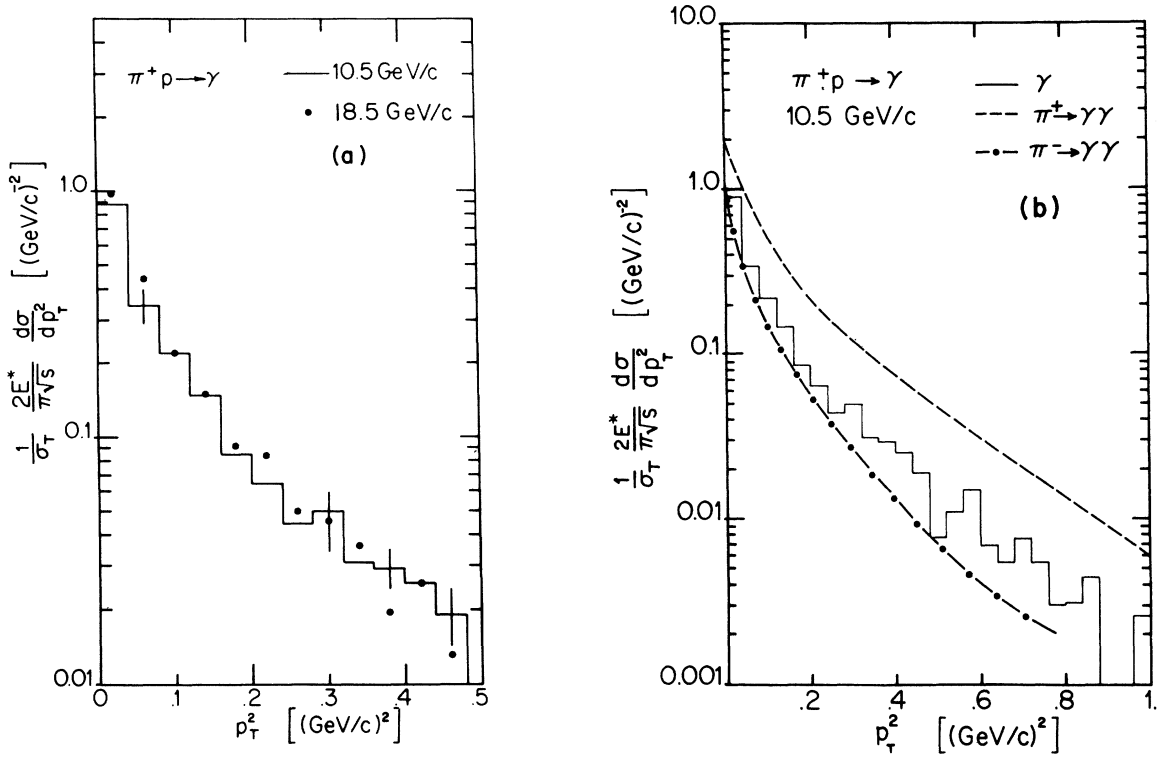

FIG. 7. Invariant differential cross section, normalized by σ_T, as a function of transverse-momentum squared for γ production in 10.5-GeV/c $\pi^+ p$ interactions: (a) compared to the results of the 18.5-GeV/c $\pi^+ p$ experiment of Ref. 12, (b) compared with the results of Monte Carlo–simulated π^0 decay using the properties of inclusive π^+ (dashed curve) and π^- (dot-dashed curve) production. Refer to text for relative normalization.

nal which accounts for all γ's to a γ excess of ~20%. The significance of these results is limited, however, by the modest number of detected γ-γ pairs.

In the two- and four-prong categories we have measured 5450 γ-γ combinations; $d\sigma/dm_{\gamma\gamma}$ is shown in Fig. 11. The smooth curve is a background estimate generated from combinations of independent γ's (taken from different events) and normalized to the data over the region $m_{\gamma\gamma} > 0.200$ GeV/c^2. To extract $\sigma(\pi^0)$, the inclusive cross section for π^0 production, we sum $d\sigma/dm_{\gamma\gamma}$ above background over the mass region 0.080 to 0.200 GeV/c^2. After a 5% correction for systematic losses, we compare this to $\sigma(\gamma)$, the inclusive γ cross section, in two- and four-prong events (see Table II):

$$\tfrac{1}{2}\sigma(\gamma) = 23.5 \pm 0.6 \text{ mb}$$

$$\sigma(\pi^0) = 21.5 \pm 2.3 \text{ mb}.$$

Thus in a comprehensive examination of all γ-γ pairs, the π^0 signal is sufficient to account for (92 + 9)% of all produced γ's. π^0 differential cross sections and $\sigma(\pi^0)$ resulting from a more detailed study of γ-γ pairs are presented in Sec. VI.

In hope of directly observing another γ source, the $m_{\gamma\gamma}$ spectrum was examined in a similar fashion in the region of the η^0, but no clear signal could be discerned. Using the few events above the estimated background and 0.38 for the fraction of η^0 decays into $\gamma\gamma$, we calculated a total η^0 inclusive cross section $\sigma(\eta^0) = (0.9 \pm 0.9)$ mb in 2- and 4-prong events. This is in contrast to the η^0/π^0 production ratios of 0.5 reported by experiments at high energies and large p_T.[18]

The measured ratio of $n_{\Lambda^0}/n_\gamma \lesssim 0.01$ implies that, even if all Λ^0's came from $\Sigma^0 \to \Lambda^0\gamma$, the Σ^0 is a negligible γ source.[19]

B. Derivation of π^0 spectra from γ spectra

From the size of the observed π^0 signal in the γ-γ mode and from the lack of other positive sources of γ's, we conclude that to ~10% accuracy all γ's come from π^0's. Having found π^0 production to be the only significant source of γ's, we can try to extract some of its properties from the γ distributions. Beginning with a paper by Sternheimer, various prescriptions[20] have been given for obtaining information about π^0 production by observing

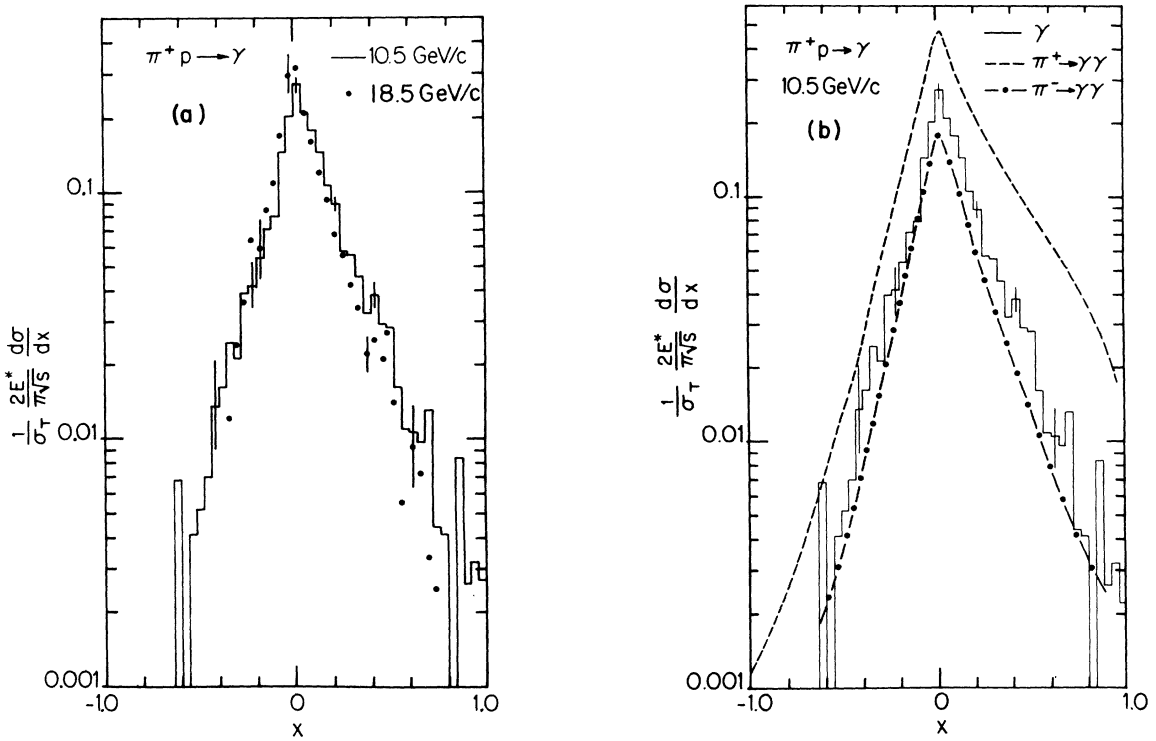

FIG. 8. Invariant differential cross section, normalized by σ_T, as a function of x for γ production in 10.5 GeV/c $\pi^+ p$ interactions: (a) compared to the results of the 18.5-GeV/c $\pi^+ p$ experiment of Ref. 12, (b) compared to the results of Monte Carlo–simulated π^0 decays using the properties of inclusive π^+ (dashed curve) and π^- (dot-dashed curve) production.

only a single γ at a time. The basic result we will use is

$$\frac{d\sigma}{dq}(\gamma) = \int_{q-m^2/4q}^{\infty} (m^2+v^2)^{-1/2} \frac{d\sigma}{dv}(\pi^0)dv, \quad q>0 \quad (5a)$$

$$= \int_{-\infty}^{q-m^2/4q} (m^2+v^2)^{-1/2} \frac{d\sigma}{dv}(\pi^0)dv, \quad q<0, \quad (5b)$$

where q = the projection of the γ's momentum on some axis, v = the projection of the π^0's momentum on the same axis, and m = mass of the π^0. This is just the familiar result that the momentum spectrum of γ's coming from an isotropic two-γ decay is composed of the sum of rectangular distributions. Equation (5) implies that the π^0 distribution can be derived by using the local derivatives of the γ spectrum. Since statistical fluctuations in the data are unrealistically magnified in taking derivatives of distributions, we prefer to use directly the integrated version given in Eq. (5). Choosing the axis parallel to the beam in the center-of-mass, we assume the following arbitrary but very general form for $(d\sigma/dx)(\pi^0)$:

$$\frac{d\sigma}{dx}(\pi^0) = f(x) = [A + B(x-x_0) + C(x-x_0)^2]\exp[-D(x-x_0) - E(x-x_0)^2]; \quad x \geq x_0 \quad (6a)$$

$$= [A + F(x_0-x) + G(x_0-x)^2]\exp[-H(x_0-x) - I(x_0-x)^2]; \quad x \leq x_0. \quad (6b)$$

For a given choice of the parameters $(A, B, \ldots, I, x_0)$, we use Eq. (5) to calculate the distribution $(d\sigma/dx)(\gamma)$. The best values for the parameters are then found by a χ^2 fit to the experimental $(d\sigma/dx)(\gamma)$ distribution. The χ^2 is defined as

$$\chi^2 = \sum_i \frac{[\sigma_m(x_i) - \sigma_p(x_i)]^2}{[\Delta\sigma_m(x_i)]^2}, \quad (7)$$

where

$\sigma_{m,p}(x_i)$ = the cross section for an interval of x, and

$\Delta\sigma_m(x_i)$ = the error in $\sigma_m(x_i)$.

The subscript m refers to the measured distribution, and p refers to that predicted from Eq. (5).

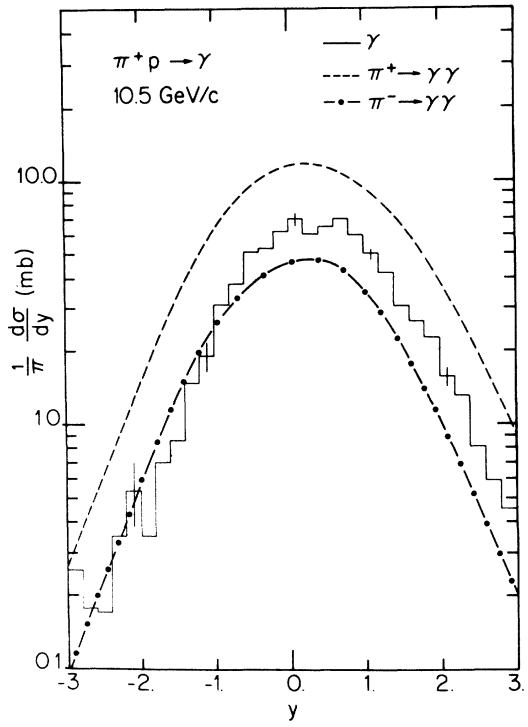

FIG. 9. Center-of-mass longitudinal rapidity distribution of γ production in 10.5-GeV/c $\pi^+ p$ interactions. The dashed (dot-dashed) curve represents the results of Monte Carlo–simulated π^0 decays using the properties of inclusve π^+ (π^-) production.

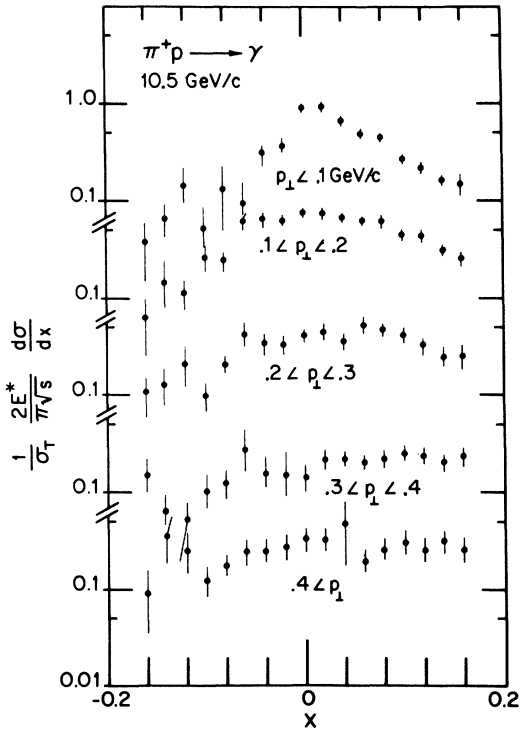

FIG. 10. The invariant differential cross section, normalized by σ_T, as a function of x for γ production in $\pi^+ p$ interactions at 10.5 GeV/c. The data is plotted separately for five intervals of transverse momentum.

This procedure has the advantage of doing a global fit using the entire γ spectrum and requiring continuity of $(d\sigma/dx)(\pi^0)$. If one merely fits a smooth function to the γ spectrum and attempts to differentiate this curve to get the π^0 distribution, difficulties arise. First, the differentiation technique cannot easily use the γ's in the interval $\frac{1}{2}(-m_{\pi^0}) \leq q \leq \frac{1}{2}(m_{\pi^0})$, since π^0's in both hemispheres contribute to this region. Second, if the two hemispheres of $(d\sigma/dx)(\gamma)$ are fitted separately, then the point $x=0$ is not well constrained and there may be incompatibilities in attempting to join the two hemispheres.

We have tested the validity of our procedure by using the pseudo-γ distributions generated from the π^+ and π^- spectra. The pseudo-γ spectra were binned analogously to the real γ's. A fit[21] of $f(x)$ given in Eq. (5) to the pseudo-γ data gave an excellent reproduction of the real π^+ and π^- $d\sigma/dx$ distributions with χ^2 probabilities of about 70% for both the π^+ and the π^-. Furthermore, Fig. 12 shows that the chosen function is easily flexible enough to assume the rather different shapes of the π^+ and π^- distributions. The actual π^0 form is not likely to be more extreme than these two examples (in fact, it appears intermediate), and the π^0 fit uses a comparable number of γ's ($\pi^0 = 7000$, $\pi^+ = 24\,000$, $\pi^- = 9000$). The $d\sigma/dx$ distribution for π^0's fits with a 20% χ^2 probability and is compared to the π^+ and π^- data in Fig. 13.[22,23]

Several interesting features of pion production are evident from the distributions shown in Fig. 13. The $d\sigma/dx$ spectrum of the π^0 falls between those of the π^+ and π^- for all x. In the projectile-fragmentation region, the ratio of π^0 to π^- is a little more than 2:1 which is characteristic of the diffractive dissociation $\pi \to 3\pi$. In the target-fragmentation region the ratio is on the order of 3:1 (with large errors) and is consistent with the diffraction dissociation of the proton. In the region near $x=0$, the π^0 shows a much greater relative increase than does the π^+ or π^-; this puzzling aspect of central pion production is not explicable in terms of either fragmentation or pionization models. We note, however, that the existence of any appreciable non-π^0 source of central γ's would significantly modify this last observation.

To convert the $d\sigma/dx$ distribution of the π^0's to $F_1(x)$, we have to weight it by the average value of $(1/\sigma_T)2E^*/\pi\sqrt{S}$ at the given x. To do this, we av-

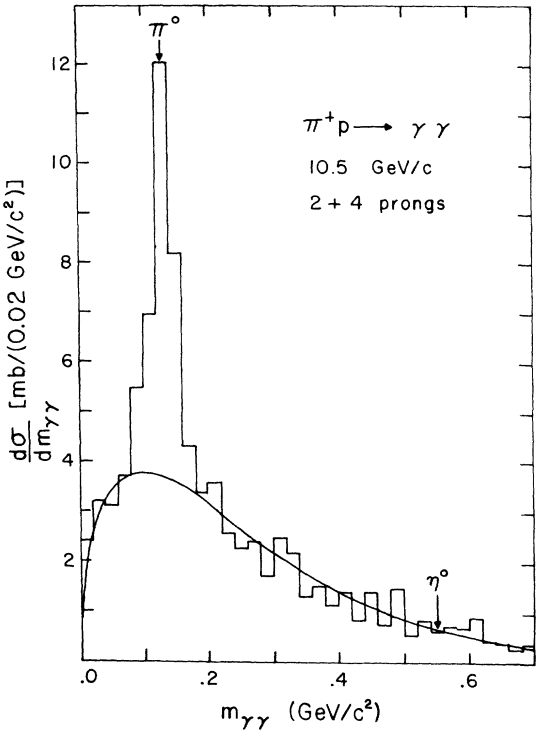

FIG. 11. The differential cross section for producing a γ-γ pair of mass $m_{\gamma\gamma}$ in 10.5-GeV/c π^+p interactions. The smooth curve represents a background generated from combinations of γ's from different events; it is normalized to the data for $m_{\gamma\gamma} > 0.200$ GeV/c^2.

erage the π^+ and π^- values (identical to ~5%) and obtain the $F_1(x)$ for π^0's shown in Fig. 14.[24] We do this for the convenience of comparison in a more widely used form although no features appear that were not evident in $d\sigma/dx$. A similar procedure reconstructs the rapidity distribution shown in Fig. 15.

$d\sigma/dx$ was also determined separately for π^0's in two- and four-prong events. The result is presented in Fig. 16 and exhibits an interesting point. The $d\sigma/dx$ distributions are very similar except in the forward region, $x > 0.5$, where the dominant contribution is from two-prong events.

Transverse momenta projected on a fixed axis can be derived in a similar manner using Eq. (5), as can p_T itself using a more complicated double integral technique. Attempts at this derivation did not seem able to improve on the results exhibited in Fig. 6, where the pseudo- γ's from simulated π^- decay are seen to give an excellent description of the p_T^2 spectrum of real γ's. The π^- can then be accepted as a good representation of the p_T^2 distribution of the π^0's.

VI. π^0 RECONSTRUCTION FROM γ-γ PAIRS

In this section we present a measurement of inclusive π^0 production obtained directly from cases in which both γ's of a π^0 decay are detected. This measurement of the π^0 spectra is essentially inde-

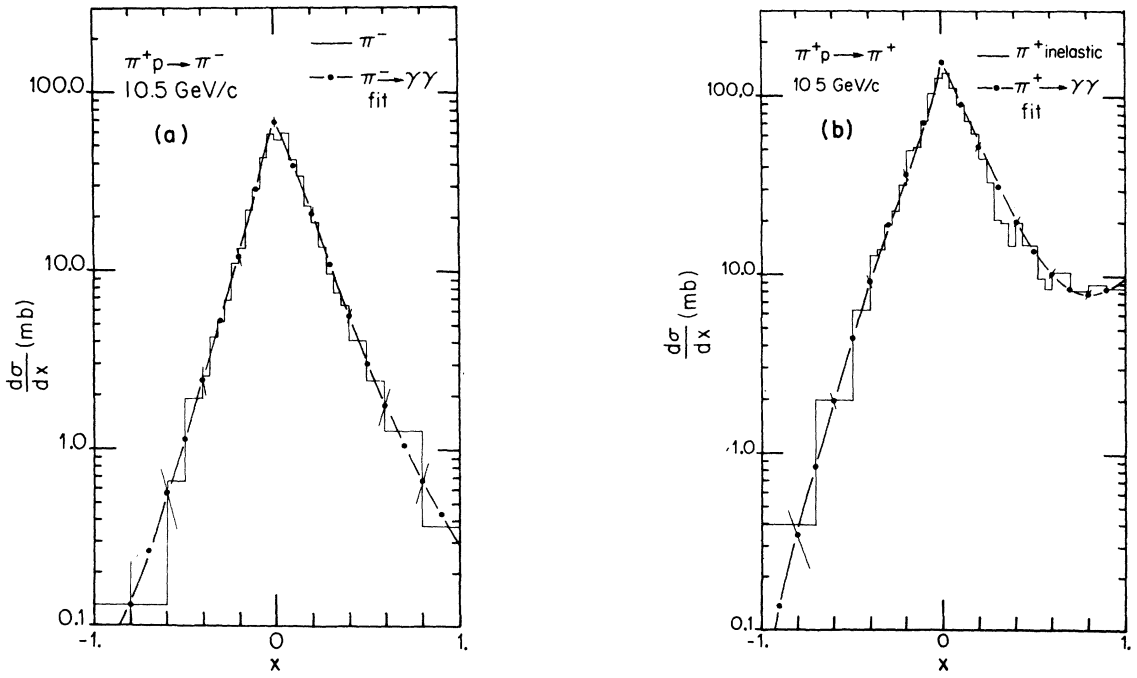

FIG. 12. The distribution $d\sigma/dx$ for (a) π^- and (b) π^+ in 10.5-GeV/c π^+p interactions. The histogram represents the measured data. The dot-dashed curve is the result obtained by applying the method of Sec. V B to the $d\sigma/dx$ distribution of pseudo-γ's generated from the charged π's via a Monte Carlo–simulated decay.

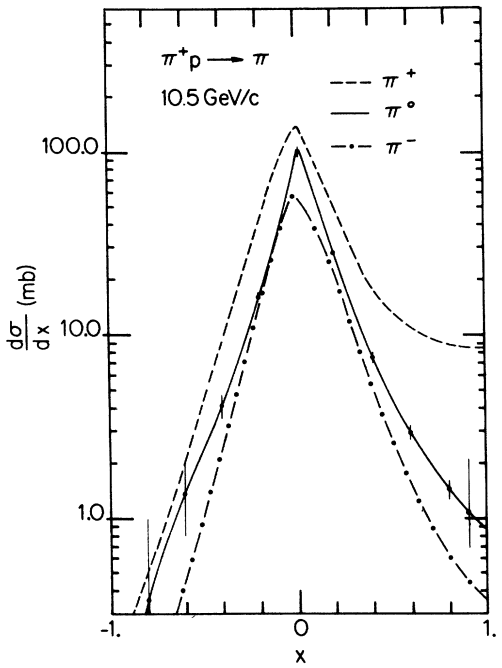

FIG. 13. Distribution of $d\sigma/dx$ for π^+ (dashed curve), π^0 (solid curve), and π^- (dot-dashed curve) production in 10.5-GeV/c π^+p interactions. Representative values are displayed for the correlated errors of the π^0 curve.

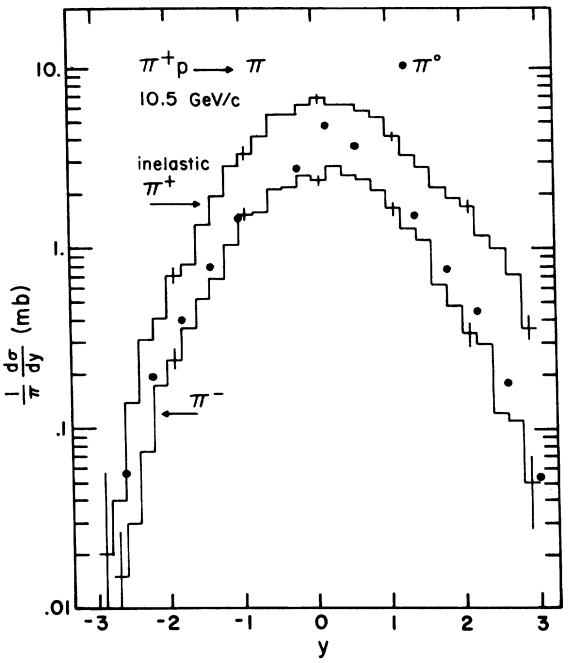

FIG. 15. Center-of-mass longitudinal rapidity distribution for π^+ (upper histogram), π^0 (solid dots), and π^- (lower histogram) production in 10.5-GeV/c π^+p interactions.

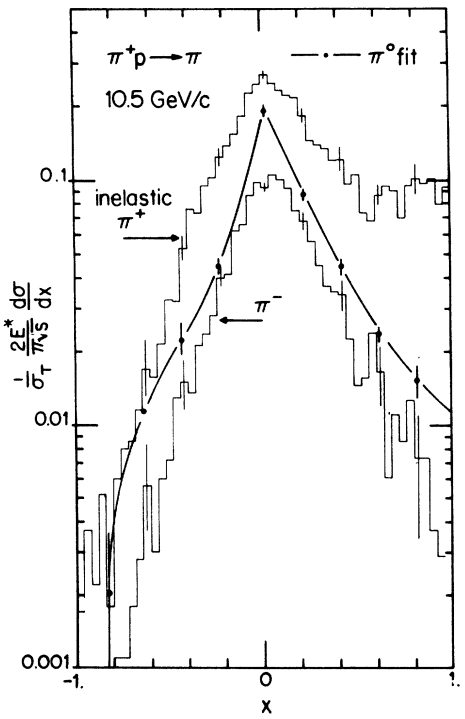

FIG. 14. Invariant differential cross section, normalized by σ_T, as a function of x for π^+ (upper histogram), π^0 (dot-dashed curve), and π^- (lower histogram) production in 10.5-GeV/c π^+p interaction.

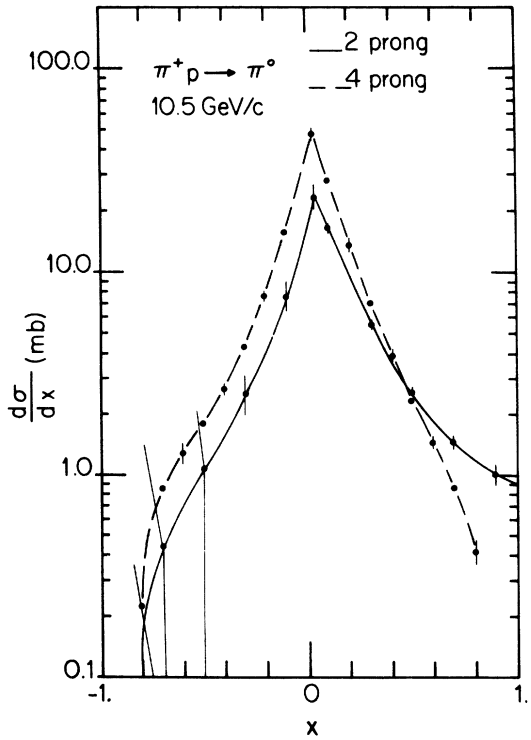

FIG. 16. The distribution $d\sigma/dx$ for π^0 production in 10.5-GeV/c π^+p interactions. The solid (dot-dashed) curve represents π^0's produced in two- (four-) prong events.

pendent of the derivation presented in Sec. V. The two-γ method is a statistically less accurate but more direct measurement of the π^0 spectrum and provides a good cross check on the inclusive γ method. We will first discuss the method used to select the $\pi^0 \to \gamma\gamma$ decays and then present the total and differential π^0 inclusive cross sections. Only two- and four-prong events are used in this analysis.

Bremsstrahlung introduces asymetrical errors in the measured momenta and angles of the conversion electrons. In considering a pair of γ's, the importance of this effect depends in a complicated way upon the energy and/or mass of the γ-γ pair. To be able to study the size of this effect simply, we have adopted a $\pi^0 \to \gamma\gamma$ selection procedure using the TVGP derived kinematic quantities, rather than performing a π^0 fit in SQUAW. The details of the method and treatment of bremsstrahlung follow.

As shown in Fig. 11, there is a rather large background under the $\pi^0 \to \gamma\gamma$ mass peak which comes from random γ-γ combinations (solid curve). We have used considerable care in extracting the π^0 candidates from this plot and correcting them for background effects. This was necessary since both the measurement width of the π^0 peak and the background level depend on the γ-γ pair energy. Therefore a simple γ-γ invariant mass cut would lead to a biased π^0 spectrum. The $\pi^0 \to \gamma\gamma$ candidates were selected by demanding that the γ-γ invariant mass was both within 60 MeV/c^2 and 2.2 measurement standard deviations of the π^0 mass. This corresponds to about a 3% probability cut for a Gaussian distribution but represents closer to a 15% π^0 loss when the effects of electron bremsstrahlung are taken into account. This loss of π^0's from the γ-γ pair candidates was studied as a function of π^0 energy using a Monte Carlo simulation which included both the bremsstrahlung energy loss of the electrons coming from the decay γ's and our electron measurement errors. We also calculated the number of background γ-γ pairs falling within both the mass cut and the probability cut. The background γ-γ mass distribution was obtained by drawing a smooth curve through the experimental γ-γ mass distribution outside the π^0 peak. This was done for each of five different γ-γ energy ranges and supplied as input to the Mone-Carlo procedure that was used to estimate the π^0 acceptance. The rejection of background within the ±60 MeV/c^2 mass cut varied from 70% at low γ-γ energies to 50% at high energies; the remaining background is

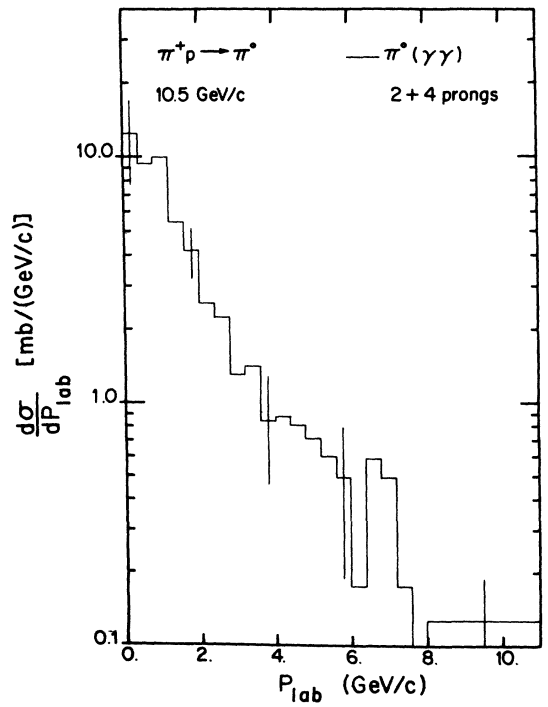

FIG. 17. The laboratory-momentum distribution of π^0's produced in two- and four-prong π^+p interactions at 10.5 GeV/c.

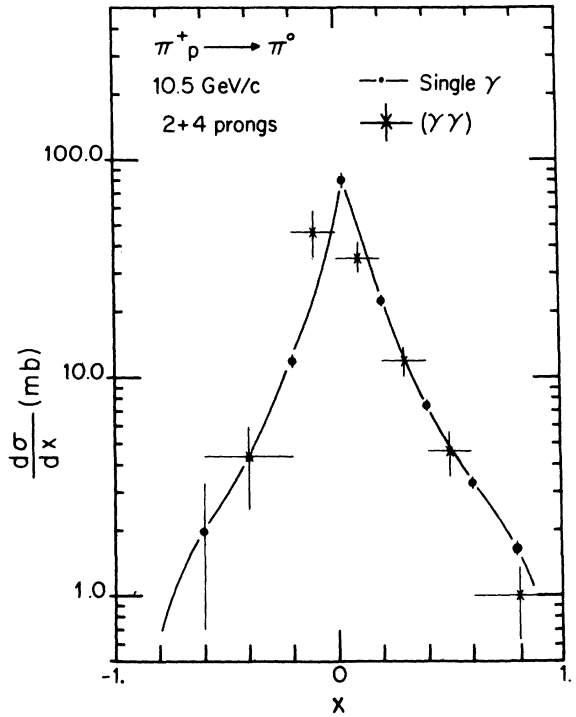

FIG. 18. The distribution $d\sigma/dx$ for π^0 production in two- and four-prong π^+p interactions at 10.5 GeV/c. The solid curve represents the results obtained from the γ inclusive distribution using the method of Sec. V B, while the starred points are from the reconstruction of π^0's from a pair of γ's. Both are normalized to the inclusive γ results.

represented by an equivalent number of γ-γ pairs from mass bins adjacent to the π^0-mass cut. By subtracting these γ-γ pairs from the selected π^0 candidates we can calculate the true π^0 spectrum in any kinematic variable.

Using this procedure, we obtain a cross section for inclusive π^0 production $\sigma(\pi^0)$, of 20 ± 3 mb. As discussed in Sec. V, if all decay γ's come from π^0 decays, then the π^0 inclusive correction is given by $\sigma(\gamma)/2$ which is 23.5 ± 0.6 mb. This is 18% higher than the directly measured value of $\sigma(\pi^0)$ but agrees within errors. Figure 17 shows the spectrum of the laboratory momentum of the π^0. In Fig. 18, we make a differential comparison of $d\sigma/dx$ (π^0) obtained directly from the γ-γ pairs to that obtained from the inclusive γ spectrum (as mentioned above, for two and four prongs only). We have normalized both cross sections to 23.5 mb for a better differential comparison. The agreement as a function of x is good except perhaps near $x = 0$, where the data allows the possibility of an additional source of γ's. We have already noted[22] the problems encountered with an excess γ's near $x = 0$ in obtaining the π^0 distribution from the γ inclusive spectrum. These difficulties, along with the present results, make the assumption that all γ's come from π^0 decays less certain near $x = 0$.

VII. DISCUSSION AND CONCLUSIONS

The aim of this experiment has been to measure the properties of γ's and π^0's produced in $\pi^+ p$ collisions at 10.5 GeV/c and to compare their properties to those of the charged π's. In the course of this study, we have determined $\langle n_0 \rangle = 1.50 \pm 0.05$ and have found $\langle n_0 \rangle$ to be nearly independent of charge multiplicity. As measured by f_2^{00}, the distributions are only slightly narrower than a Poisson distribution ($f_2^{00} = -0.05 \pm 0.06$). Again, these properties do not depend strongly on the charge multiplicity.

The γ spectra agree well with other data in the same energy region, but a 30–40% deviation from scaling is seen when $F_1(x = 0)$ or $(1/\sigma_{\text{inel}}) d\sigma/dy \big|_{y=0}$ are compared to higher-energy data. When $F_1(x)$ is plotted for several restricted p_T regions, the factorization of the invariant cross section into independent functions of p_T^2 and x is found to fail. Pseudo-γ's generated from π^-'s via a Monte-Carlo procedure indicate that the p_T^2 distributions of π^- and π^0 are nearly identical.

We find that, within an uncertainty of 10%, all of the observed γ's come from the decay $\pi^0 \to \gamma\gamma$.

$(d\sigma/dx)(\pi^0)$ has been extracted from the γ distribution. Over the entire x interval we find that $(d\sigma/dx)(\pi^-) < (d\sigma/dx)(\pi^0) < (d\sigma/dx)(\pi^+)$. Further, the following is found: (1) The π^0 production rate approaches that of the π^+ in the target region; (2) at $x = 0$ the π^+, π^0, and π^- cross sections have not reached the asymptotic equality predicted by Mueller-Regge theory[25] although the π^0 value favors that of the π^+; (3) in the projectile region, the π^0 follows the nonleading π^- except for a small π^0 enhancement in 2-prong events.

An independent determination of $(d\sigma/dx)(\pi^0)$ has been made from detected γ-γ pairs. Good agreement between this measurement and that derived from the single-γ data is found over the entire range of Feynman x. This constitutes a differential confirmation of π^0's as the overwhelming γ source.

In summary, the π^+, π^0, and π^- spectra are found to be approximately similar in form, the π^0 value being bounded by the π^+ and π^- values over the entire kinematic interval. Differences in the magnitude of the distributions exist as do local variations in the shapes. Further detailed experiments at higher energies would be interesting in order to study the continued existence and energy dependent nature of these differences.

ACKNOWLEDGMENTS

We thank R. Gearhart and J. Murray for their help with the pion beam, and R. Watt and the 82-inch bubble-chamber crew for their valuable assistance during the data run. We are especially grateful for the diligent efforts of our scanning staff.

---

*Work supported by the U. S. Energy Research and Development Administration, Contract No. E-(40-1)-3065.

†Work based in part on the disssertation submitted by J. R. Elliott to the Duke University Graduate School in partial fulfillment of the requirements for the Ph.D. degree.

‡Present address: Physics Department, University of Illinois, Urbana, Illinois, 61801.

§Present address: Computation Center, University of North Carolina, Chapel Hill, North Carolina, 27514.

||Present address: Physics Department, University of Massachusetts, Amherst, Massachusetts, 01002.

[1]Reviews of single-particle inclusive data have been given by L. Van Hove, Phys. Rep. 1C, 347 (1971); W. R. Frazer *et al.*, Rev. Mod. Phys. 44, 284 (1972); L. Foà, Phys. Rep. 22C, 1 (1975).

[2]For a survey of inclusive γ and π^0 results, see J. R. Elliott, Ph.D. dissertation, Duke University, 1976 (unpublished).

[3]Very-low-energy electron pairs suffered larger losses in both scanning and measuring. To maintain a well-defined sample, a strict rejection was made for $E_\gamma < 30$ MeV; this eliminated the region of strong biases. A Monte Carlo simulation with π^- indicates a loss of 2.5% of the γ's by this cut. This was corrected for in the γ and π^0 cross sections and in the extraction of the

π^0 spectra but was neglected elsewhere.

[4]L. Behr and P. Mittner, Nucl. Instrum. Methods 20, 446 (1963); D. Morollet, Ecole Normale Superieure Laboratoire de l'Accelerateur Lineaire Orsay Report No. L. A. L. 1190, 1968 (unpublished).

[5]For details of this and other aspects of the γ processing, see Ref. 2.

[6]G. A. Akopdjanov *et al.*, Nucl. Phys. B75, 401 (1974).

[7]W. M. Yeager, Ph.D. dissertation, Duke University, 1976 (unpublished); W. M. Yeager *et al.*, Phys. Rev. D 16, 1294 (1977).

[8]For convenience we define some standard inclusive cross sections. First we express the invariant cross section in the center-of-mass frame $E^* d^3\sigma/d^3\vec{p}$ as $f(x,p_T{}^2,s)$, a structure function of the Feynman variable $x = p_\parallel^*/p_{\max}^*$ and the transverse momentum p_T:

$$f(x,p_T{}^2,s) = \frac{2E^*}{\pi\sqrt{s}} \frac{d\sigma}{dx dp_T{}^2};$$

then

$$F_1(x) = \frac{1}{\sigma_T} \int_0^\infty f(x,p_T{}^2,s)\, dp_T{}^2$$

and

$$F_2(p_T{}^2) = \frac{1}{\sigma_T} \int_{-1}^{+1} f(x,p_T{}^2,s) dx.$$

[9]J. T. Powers *et al.*, Phys. Rev. D 8, 1947 (1973).

[10]M. E. Binkley *et al.*, Phys. Lett. 45B, 295 (1973).

[11]$f_2^{00} = \frac{1}{4}(f_2^{\gamma\gamma} - \langle n_\gamma \rangle)$, where $f_2^{\gamma\gamma} = \langle n_\gamma (n_\gamma - 1)\rangle - \langle n_\gamma \rangle^2$. See G. H. Thomas and B. R. Webber, Phys. Rev. D 9, 3113 (1974).

[12]N. N. Biswas *et al.*, Phys. Rev. D 10, 3579 (1974).

[13]J. Erwin *et al.*, Phys. Rev. Lett. 35, 142 (1975); D. Bogert *et al.*, Report No. NAL Conf. 74/55-EXP (unpublished).

[14]G. Charlton *et al.*, Phys. Rev. Lett. 29, 1759 (1972).

[15]O. Balea *et al.*, Nucl. Phys. B52, 414 (1973); B63, 114 (1973); B83, 365 (1974); N. Angelov *et al.*, Yad. Fiz. 21, 166 (1975) [Sov. J. Nucl. Phys. 21, 87 (1975)]; L. Gerdyukov *et al.*, Yad. Fiz. 21, 147 (1975) [Sov. J. Nucl. Phys. 21, 76 (1975)].

[16]R. N. Cahn, Phys. Rev. D 7, 247 (1973); G. R. Farrar and S. C. Frautschi, Phys. Rev. Lett. 36, 1107 (1976).

[17]J. H. Campbell *et al.*, Phys. Rev. D 8, 3824 (1973); D. Swanson *et al.*, Phys. Lett. 48B, 479 (1974); F. Pierre *et al.*, Nucl. Phys. B77, 45 (1974); P. Beilliere *et al.*, *ibid.* B91, 219 (1975).

[18]F. W. Büsser *et al.*, Phys. Lett. 55B, 232 (1975); K. Eggert *et al.*, Nucl. Phys. B98, 49 (1975).

[19]From our measurement of Λ^0 or as in P. H. Stuntebeck *et al.*, Phys. Rev. D 9, 608 (1974).

[20]R. M. Sternheimer, Phys. Rev. 99, 277 (1955); R. G. Glasser, Phys. Rev. D 6, 1933 (1972), 8, 3223 (1973); G. I. Kopylov, Nucl. Phys. B52, 126 (1973).

[21]F. James and M. Roos, CERN Computer Program Library Report No. D506 (unpublished).

[22]In this procedure the γ bin $0.00 < x < 0.01$ was smoothed to a value consistent with neighboring bins. The unsmoothed result had a 15% γ excess which was incompatible with a π^0 source.

[23]Note that in all displays of the π^0 fit the errors are correlated. The points with error bars are chosen to show representative values.

[24]For $F_1(x)$ of the π^0, the errors include the uncertainty in the average value of $(1/\sigma_T) 2E^*/\pi\sqrt{s}$ (from the π^+/π^- data) at a given value of x, as well as the uncertainty in $(d\sigma/dx)(\pi^0)$.

[25]A. H. Mueller, Phys. Rev. D 2, 2963 (1970).